Research Article

Tong Wu, Ruidong Yang*, Junbo Gao, and Jun Li

Age of the lower Cambrian Vanadium deposit, East Guizhou, South China: Evidences from age of tuff and carbon isotope analysis along the Bagong section

https://doi.org/10.1515/geo-2020-0287
received August 12, 2020; accepted July 22, 2021

Abstract: The early Cambrian is a critical interval of dramatic oceanic and biochemical changes in geological history. The black shale deposits, which are rich in Mo, Ni, V, and platinum group elements (PGE), are a reflection of that interval. Among all known Cambrian black shale deposits in South China, the vanadium deposits are poorly constrained by geochronology. The newly discovered tuff layer in the Sansui Bagong vanadium deposit in Guizhou Province can provide excellent constraints on the age of vanadium deposits. In this study, we obtain a new zircon U–Pb isotopic age, which can constrain the age of the vanadium deposit. This tuff occurs in the middle part of the ore bed, and the age of the tuff layer can reflect the mineralization age of the V deposit. Laser ablation inductively coupled plasma mass spectrometry (LA-ICP-MS) is used in this study to obtain the zircon U–Pb age of the tuff and indicates that the event of volcanic activity took place at 520.9 ± 1 Ma. This age is close to the boundary between the Cambrian Terreneuvian and Series 2. This result provides a good constraint on the age of the vanadium deposits in South China and makes the vanadium deposits to be comparable with other Mo–Ni–PGE deposits. The alteration of organic carbon isotope ($\delta^{13}C_{org}$) values can reflect changes in the marine environment and is widely used in stratigraphic correlation. The analysis of the $\delta^{13}C_{org}$ values of the ore bed in the present study reveals a positive excursion at the bottom of the deposit and a negative excursion in the V-enriched layer. The $\delta^{13}C_{org}$ values in the Bagong section are comparable to those in the Xiaotan and Longbizui sections. The ages of the Sansui vanadium deposit constrained by the U–Pb isotopic age of the tuff and the $\delta^{13}C_{org}$ values are consistent. All of the data lead us to infer that the vanadium deposit formed at approximately 521 Ma.

Keywords: vanadium deposit, Zircon, U–Pb isotope, organic carbon isotope, black shale, Cambrian

1 Introduction

South China is an ideal area for studying changes in marine environment and early biological evolution because of the wide distribution of strata and abundant fossils from the Precambrian-Cambrian Period in this region. The lower Cambrian black shales are an important ore-bearing layer rich in Mo, Ni, V, U, and other elements. Great insights into palaeontology and palaeo-marine environments have been achieved through studies of the lower Cambrian strata in this area [1–10]. However, a number of geological problems, such as the location of the Precambrian-Cambrian boundary and the relative ages of some layers, have not been fully solved [11–15].

Black shale vanadium deposits are widely distributed in the lower Cambrian strata of South China [10,16]. The metallogenic belt of these deposits extends from northeastern Yunnan Province to southwestern Hubei Province [10,16–18]. The lithology of the vanadium-enriched black shales is stable; it is an ideal correlation stratum as a making layer. The metallogenic age of V deposit is a relatively complex and controversial issue in the study of earl Cambrian. Through division and contrast of metallogenic sequence, Li et al. indicated that the age of V deposit is

* **Corresponding author: Ruidong Yang,** Guizhou University, Resource and Environmental Engineering College, Guiyang, 550025, Guizhou Province, China, e-mail: rdyang@gzu.edu.cn
Tong Wu: Guizhou University, Resource and Environmental Engineering College, Guiyang, 550025, Guizhou Province, China; Henan University of Engineering, Resource and Environmental College, Zhengzhou, 450000, Henan Province, China
Junbo Gao, Jun Li: Guizhou University, Resource and Environmental Engineering College, Guiyang, 550025, Guizhou Province, China

more than Mo–Ni deposits [19]. Wei et al. thought that the mineralization of vanadium began earlier than that of Mo–Ni, but the end of mineralization may have occurred later than Mo–Ni deposits [20]. The studies of Mao et al. (2002) and Jiang et al. (2003) showed the age of Mo–Ni–PGE is 541 ± 16 and 537 ± 10 Ma, respectively. Some newer studies have found that the age of Mo–Ni deposits is about 521 Ma [21,22]. By the study of Mo–Ni–V–PGE-enriched layer at Hunan and Guizhou, Fu et al. indicated that the age of Mo–Ni–V-enriched layer is 520.3 ± 9.1 Ma [23]. It can be seen that there is a lack of data on the age of V deposit.

In this study, new zircon U–Pb age data were obtained by analysing zircons from a newly discovered tuff layer in the Bagong V deposit. The tuff is located in the middle part of the V-enriched layers, and this is the first study with a direct evidence about the age of V-enriched layers in South China.

2 Geological setting

The tectonic setting of the southern and eastern Yangtze Platform in the early Cambrian was a passive continental margin, and the seawater depth gradually increased from northwest to southeast [1,4,27]. Three facies belts can be distinguished based on water depth and sedimentary rocks on the Yangtze Platform, South China. From northwest to southeast, the sequence of sedimentary facies is a shallow platform, continental slope, and deep-water basin (see Figure 1a). The sedimentary facies of East Guizhou included continental slope facies and deep-water basin.

In the study area, the strata from old to young are the Ediacaran Nantuo Formation and Doushantuo Formation Liuchapo Formation (lower part), and the Cambrian Liuchapo Formation (upper part), Jiumenchong Formation, Bianmachong Formation, and Balang Formation (see Figure 1b). The rocks that can be seen in the Bagong section represent the Doushantuo Formation, Liuchapo Formation, and Jiumenchong Formation. The lower part of the Doushantuo Formation comprises mainly dolomite, and the upper part is black shale, which contains the Wonghui biota. The Liuchapo Formation is a diachronous unit from the Ediacaran to the lower Cambrian; it is composed of siliceous rocks in the lower to middle part and of carbonaceous shale and siliceous rocks in the upper part. The Jiumenchong Formation is in conformable contact with the underlying Liuchapo Formation. Jiumenchong Formation is also named the Niutitang Formation in Hunan and northern Guizhou. The Niutitang Formation is composed mainly of carbonaceous shale and is the position where the earliest trilobites appear [14,25]. The

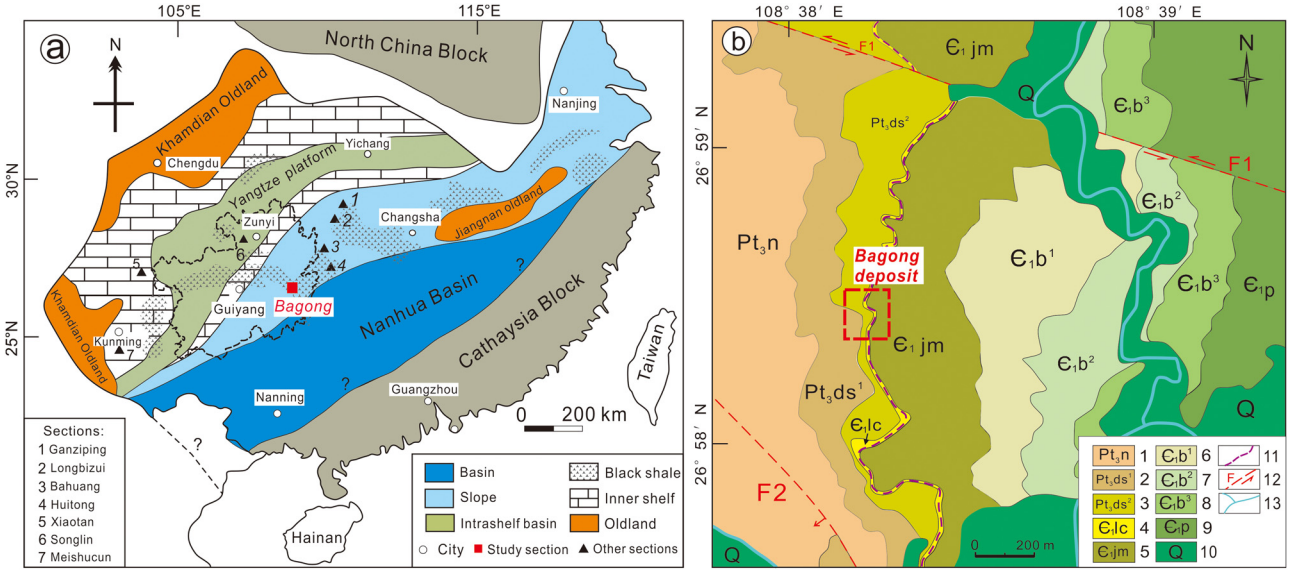

Figure 1: (a) Palaeogeography of the Early Cambrian in the Yangtze block, South China. (modified after [24,26]). (b) Geological map of the study area. 1. Ediacaran Nantuo Formation; 2. Member 1 of Ediacaran Doushantuo Formation; 3. Member 2 of Ediacaran Doushantuo Formation; 4. Cambrian Liuchapo Formation; 5. Cambrian Jiumenchong Formation; 6. Member 1 of Cambrian Bianmachong Formation; 7. Member 2 of Cambrian Bianmachong Formation; 8. Member 3 of Cambrian Bianmachong Formation; 9. Cambrian Balang Formation; 10. Quaternary; 11. Outcrop line of vanadium ore bed; 12. Fault; 13. River.

Mo–Ni-enriched layer is located at the bottom of the Niutitang Formation, and the vanadium deposits are found in the upper Liuchapo Formation.

An important metallogenic belt of Ni–Mo–V-platinum group elements (PGE) developed in South China. This metallogenic belt is associated with the black shale and extends for up to 2,000 km from northeast to southwest [28]. The Bagong vanadium deposit is located 2 km west of Sansui County, eastern Guizhou Province. Mainly, Ediacaran and Cambrian strata are exposed in this area (see Figure 1b). The vanadium deposit occurs in the upper Liuchapo Formation, with a thickness of 2–3 m (see Figure 2a). Many phosphorous nodules can be observed in the roof of the deposit (see Figure 2b). The vanadium deposit is associated with specific rocks, including siliceous rocks, carbonaceous rocks, and phosphorous nodules. Among them, the siliceous rocks and the phosphorus nodules are surrounding rocks of seam and the carbonaceous shale is the ore. The siliceous rocks in the deposit are lenticular, wedge-shaped, or stratiform, and the vanadium-rich carbonaceous shales are interbedded with the siliceous rocks.

3 Methods

Tuff samples were collected in the Bagong vanadium deposit, Sansui, Guizhou Province. The sample location was approximately 70 cm below the Jiumenchong Formation carbonaceous shale and 1.5 m above the underlying Doushantuo Formation limestone (see Figure 2a and c). Contamination by the surrounding rock fragments was strictly avoided during sample collection. In total, 15 kg of tuffaceous material was collected. Zircons were separated from the tuffaceous samples using standard gravitational separation techniques. Zircon grains were handpicked under a binocular microscope, and only grains without cracks and inclusions were selected.

These grains were mounted in epoxy resin and then polished to expose the crystals for analysis. Internal structures were examined and imaged using cathodoluminescence (CL) prior to inductively coupled plasma mass spectrometry (ICP-MS) analyses. The CL imaging was completed at Chongqing Yujin Technology Co., Ltd.

Zircon U–Pb isotope measurements were completed at Nanjing FocuMS Technology Co., Ltd. The laser ablation

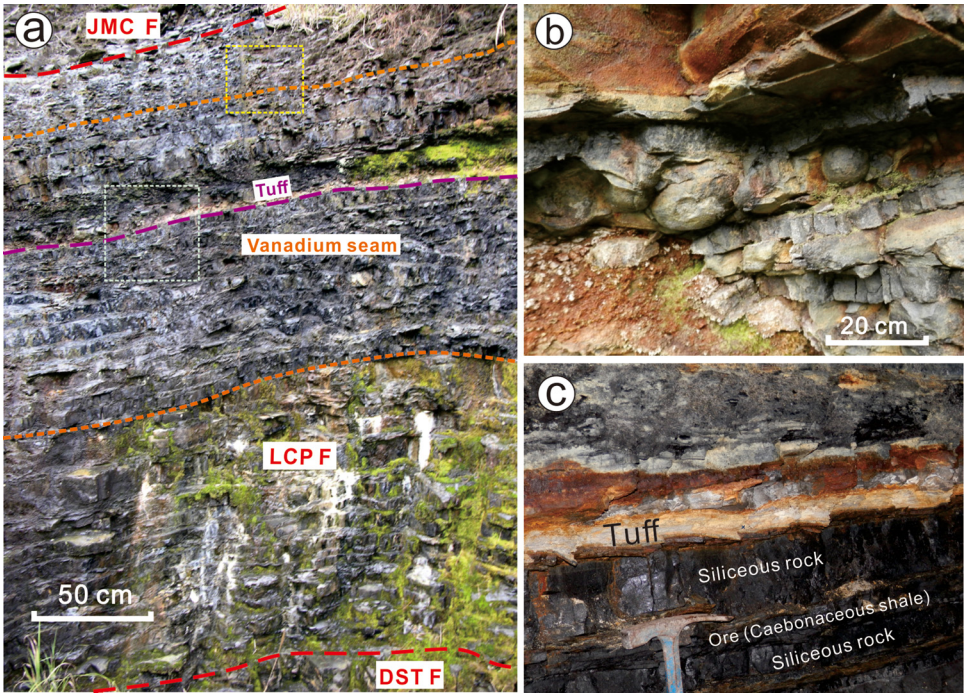

Figure 2: Field photographs of the V-rich black shale in the Liuchapo Formation, Guizhou Province. (a) The vanadium seam (in the area between two orange dotted lines) is located in the Liuchapo Formation (LCP F), which is mainly composed of siliceous rocks with thin-bedded carbonaceous shales. The red dotted lines mark the boundary of formations. DST F = Doushantuo Formation; JMC F = Jiumenchong Formation. The violet dotted line marks the layer of tuff. (b) Many phosphorous nodules can be observed in the roof of deposit. (c) The tuff in the Bagong vanadium deposit, Guizhou. This is the sampled layer for testing in present study. The positions of (b) and (c) are shown in yellow (b) and green (c) boxes in (a).

was performed with a Geo-Las Pro 193 nm ArF excimer laser made by Lamda Physik, and the ICP-MS was performed with an Agilent 7700× instrument. The energy density of the ultraviolet laser was 5.12 J/cm^2, the diameter was 33 μm, the frequency was 6 Hz, and the time of laser ablation was 40 s. Zircon aerosols were introduced into the mass spectrometer by helium for analysis. Euhedral zircons free of inclusions and cracks, commonly with clear oscillatory rims, were selected for age measurements. Zircon 91500 was used as primary standard reference material, and GJ-1 (600 Ma) and Plesovice (337 Ma) zircons were used as blind samples. The calibration of the Pb content in the zircons was conducted by applying Si as an internal standard and SRM610 as the primary standard reference material. In addition, Zr was used as an internal standard to calibrate other trace elements in the zircons [27,29]. The raw data were analysed using ICPMSDataCal [30,31]. The zircon U–Pb concordia age diagram and average weight calculation of ages were processed using Isoplot 3.0 [31].

The uncertainty of laser ablation ICP-MS (LA-ICP-MS) zircon U–Pb dating is approximately 4% (2RSD) [32,33]. However, this value is the external error obtained using the same experimental method. The accuracy of sensitive high-resolution ion microprobe (SHRIMP) analysis is higher than LA-ICP-MS in determinations of single zircon ages, but the U–Pb concordia ages are nearly consistent between the methods [34]. For the simple-genesis zircons in this study, by increasing the number of test points and using a narrow laser ablation beam, an acceptable accuracy of LA-ICP-MS was obtained.

The Th, U, and TOC content tests were completed at the ALS Minerals-ALS Chemes, Guangzhou, China. The analysis of Th and U contents was performed with ICP-MS61 method. The data of TOC content based on the calculation of loss on ignition (LOI) samples were ground to 200 mesh powder and were dried at 110°C for 2 h, and then calcined at 500°C for 4 h. The weight difference between the calcined and after is the LOI. The conversion relationship between LOI and TOC is:

$$W_{(\mathrm{TOC})} = \frac{\mathrm{LOI}}{2.125}$$

The conversion factor between LOI and TOC that we used in this study is 2.125; this conversion factor is based on the study of traditional conversion relationship between LOI and TOC in shale by Qiu et al. [35]; the relative error is less than 2% [35].

The $\delta^{13}C_{org}$ analysis was completed at the Institute of Geochemistry, Chinese Academy of Sciences. The samples for $\delta^{13}C_{org}$ analysis were ground into powder together with the samples used for element content determination. The $\delta^{13}C_{org}$ values were analysed with a ThermoFisher MAT 253 isotope mass spectrometer. The results are presented in Table 2, and the sampling locations can be seen in Figure 5.

4 Results

Most of the zircon grains from the tuff in the Sansui vanadium deposit have high transparency under a microscope

Table 2: Organic carbon and oxygen isotopes and selected redox proxies record of the Bagong section

Sample	$\delta^{13}C_{org}$ (‰ VPDB)	std error*t (‰)	U (ppm)	Th (ppm)	Th/U	LOI (wt%)	TOC (wt%)
SH-16	−33.62	0.021	30	20	0.67	14.01	6.59
SH-15	−33.81	0.033	70	20	0.29	8.92	4.20
SH-14	−33.77	0.019	50	<20	<0.4	16.44	7.74
SH-13	−33.83	0.031	20	<20	<1	8.72	4.10
SH-12	−33.86	0.008	40	20	0.5	14.59	6.87
SH-11	−33.41	0.005	50	<20	<0.4	3.71	1.75
SH-10	−33.08	0.018	80	<20	<0.25	2.17	1.02
SH-9	−33.49	0.007	80	<20	<0.25	23.52	11.07
SH-8	−31.58	0.027	10	<20	<2	2.34	1.10
SH-7	−31.79	0.009	40	<20	<0.5	11.83	5.57
SH-6	−30.63	0.012	10	<20	<2	3.01	1.42
SH-5	−30.97	0.018	<10	<20	—	32.02	15.07
SH-4	−30.04	0.009	10	<20	<2	35.15	16.54
SH-3	−30.86	0.024	310	<20	<0.06	42.83	20.16
SH-2	−31.01	0.024	20	<20	<1	24.37	11.47
SH-1	−31.2	0.015	80	<20	<0.25	3.15	1.48

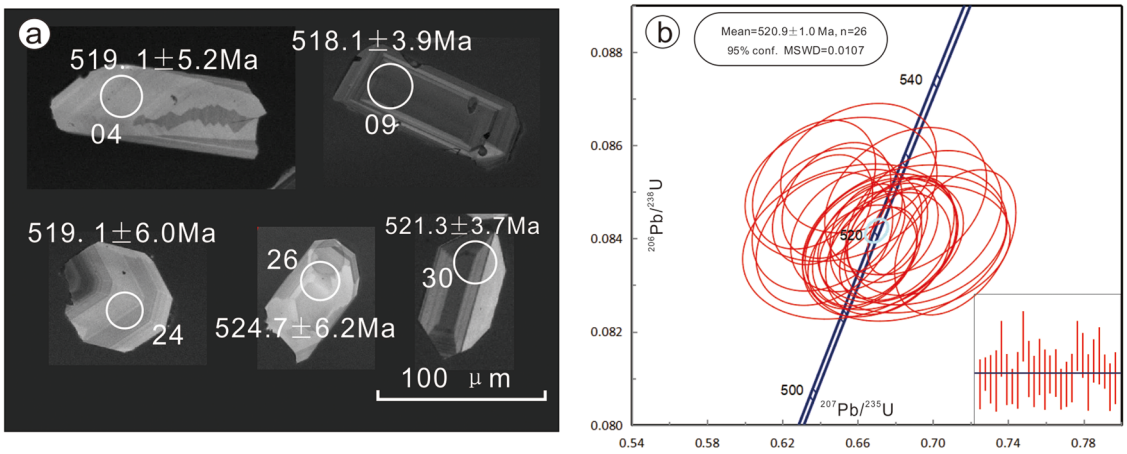

Figure 3: (a) CL images of zircons from the tuff layer, Bagong, Guizhou. The circles are LA-ICP-MS analytical spots. (b) U–Pb concordia diagrams of zircon analyses from Bagong; The weighted mean age. Weighted mean $^{206}Pb/^{238}U$ ages are shown at the 95% confidence level for the main group of zircons. (MSWD: mean square weighted deviation).

and a pale yellow to light brown colour. Most of the zircons are short, columnar, and idiomorphic, with lengths of 50–140 μm, widths of 30–60 μm, and length-width ratios of 1:1–2.5:1 (see Figure 3a). The zircons in the tuff have variable Th and U contents; thus, the CL images differ in intensity. Some zircons are darker; most of them are brighter in the CL images. Most exhibit primary oscillatory zoning in the CL images, and the Th/U ratios of all concordant zircons are greater than 0.4, which indicates a magmatic origin. All of the points located for the test were in obvious oscillatory zones. Thirty two points were tested, which have a concordance of more than 90%. The evaluation results and age calculations are provided in Table 1. The U–Pb concordia ages of the zircons are shown in Figure 3. Points with greater than 95% concordance were adopted (points L0269-06 and 27 were deducted); point L0269-01 has abnormally high Th and U contents, which may represent contamination, so the data were excluded. The zircon U–Pb ages from the tuff in the Sansui vanadium deposit are within the range of 507.1–528.9 Ma, with an isochron age of 520.9 ± 1.0 Ma (see Figure 3b). There were 26 points in conformity after common ^{204}Pb correction [36] (points L0269-12, 28, and 29 were removed).

The TOC content is high in most samples from the Bagong section, ranging from 1.06 to 20.16%. Variation range of $\delta^{13}C_{org}$ content is from −30.04 to −33.86‰ and decreases gradually from the bottom to the top along the section; the maximum top-bottom difference is 3.82‰. The ratio of Th/U is <1 in most samples. The results of $\delta^{13}C_{org}$ and element are provided in Table 2.

5 Discussion

5.1 Effects of post-diagenesis on $\delta^{13}C_{org}$

The $\delta^{13}C_{org}$ values of sediments may be altered by microbial degradation in the early diagenetic stage and by late thermal metamorphism. The values of $\delta^{13}C_{org}$ in sediments decrease slightly in the early diagenetic stage, but by less than 1–2‰ [37–41]. Hydrocarbons rich in ^{12}C are preferentially decomposed when sedimentary rocks are affected by later thermal metamorphism. As a result, the $\delta^{13}C_{org}$ of residual organic matter increases by less than 2‰ [42,43]. Compared with the time of deposit formation, the duration of volcanic eruptions is short and thus has little effect on the $\delta^{13}C_{org}$ values of the entire deposit. The correlation between the $\delta^{13}C_{org}$ values and TOC contents in the Bagong vanadium deposit is low ($R^2 = 0.1593$), which indicates the $\delta^{13}C_{org}$ values were not obviously transformed post-diagenesis (see Figure 4).

5.2 Stratigraphic correlation framework of the Yangtze platform established by $\delta^{13}C_{org}$

In addition to U–Pb aging, carbon and oxygen isotope analyses are effective methods to establish stratigraphic correlations. From the late Ediacaran to the Cambrian, the carbon and oxygen isotopes of the global marine biota fluctuated significantly [44–52]. Two significant

Table 1: Zircon U–Pb isotope data of tuff from the Bagong vanadium deposit, Guizhou

Sample No.	Content (ppm)			Ratio										Age (Ma)						Concordance (%)
	Pb	U	Th	Th/U	$^{207}Pb/^{206}Pb$	±	$^{207}Pb/^{235}U$	±	$^{206}Pb/^{238}U$	±	$^{208}Pb/^{232}Th$	±	$^{207}Pb/^{206}Pb$	±	$^{207}Pb/^{235}U$	±	$^{206}Pb/^{238}U$	±	$^{208}Pb/^{232}Th$	±	
L0269-01[1]	31.83	464.77	663.13	0.70	0.0527	0.0010	0.2765	0.0054	0.0382	0.0003	0.0130	0.0002	322.3	16.7	247.9	4.3	241.6	2.1	260.4	3.8	97
L0269-02	5.02	30.50	47.74	0.64	0.0605	0.0029	0.6903	0.0334	0.0838	0.0009	0.0281	0.0008	633.4	100.9	533.0	20.1	518.6	5.4	559.8	15.2	97
L0269-03	36.01	222.32	345.98	0.64	0.0585	0.0009	0.6812	0.0105	0.0841	0.0006	0.0264	0.0003	550.0	33.3	527.5	6.4	520.8	3.6	526.2	6.5	98
L0269-04	7.23	42.05	69.59	0.60	0.0590	0.0023	0.6775	0.0255	0.0840	0.0009	0.0280	0.0007	568.6	83.3	525.3	15.5	519.7	5.2	558.5	13.2	98
L0269-05	4.22	27.84	40.06	0.69	0.0607	0.0034	0.6849	0.0359	0.0839	0.0011	0.0259	0.0008	629.3	120.4	529.8	21.6	519.4	6.6	516.6	16.5	98
L0269-06[2,3]	4.70	26.36	45.67	0.58	0.0645	0.0036	0.7401	0.0405	0.0848	0.0011	0.0258	0.0010	766.7	118.5	562.4	23.6	524.9	6.7	515.1	18.8	93
L0269-07	6.54	47.65	59.82	0.80	0.0558	0.0029	0.6511	0.0337	0.0851	0.0010	0.0270	0.0007	455.6	119.4	509.2	20.7	526.2	6.1	538.0	14.5	96
L0269-08	5.82	43.10	53.40	0.81	0.0600	0.0028	0.6922	0.0309	0.0840	0.0009	0.0272	0.0006	605.6	100.0	534.1	18.5	519.7	5.4	542.9	12.4	97
L0269-09	28.95	177.39	279.36	0.63	0.0578	0.0012	0.6710	0.0137	0.0837	0.0006	0.0269	0.0004	520.4	44.4	521.3	8.3	518.1	3.9	536.3	7.7	99
L0269-10	12.69	59.98	139.33	0.43	0.0617	0.0018	0.7118	0.0213	0.0839	0.0010	0.0291	0.0007	664.8	56.5	545.8	12.6	519.5	6.1	580.4	13.1	95
L0269-11	7.45	57.51	67.45	0.85	0.0567	0.0023	0.6604	0.0273	0.0855	0.0009	0.0256	0.0006	479.7	90.7	514.9	16.7	528.9	5.4	510.8	11.0	97
L0269-12[3]	6.42	48.60	60.67	0.80	0.0588	0.0025	0.6681	0.0283	0.0823	0.0009	0.0246	0.0006	566.7	94.4	519.5	17.2	509.8	5.6	491.6	11.7	98
L0269-13	6.18	44.68	56.23	0.79	0.0608	0.0025	0.6951	0.0273	0.0843	0.0010	0.0268	0.0006	631.5	89.6	535.8	16.4	521.9	6.1	535.4	12.5	97
L0269-14	7.54	57.05	68.42	0.83	0.0593	0.0025	0.6726	0.0268	0.0839	0.0009	0.0267	0.0006	588.9	91.5	522.3	16.3	519.3	5.6	532.2	10.9	99
L0269-15	6.22	47.24	56.67	0.83	0.0558	0.0023	0.6438	0.0263	0.0844	0.0010	0.0252	0.0006	455.6	125.0	504.7	16.3	522.4	6.0	502.6	11.5	96
L0269-16	5.10	40.06	45.75	0.88	0.0577	0.0034	0.6560	0.0377	0.0839	0.0011	0.0266	0.0007	520.4	129.6	512.2	23.1	519.6	6.5	530.8	13.9	98
L0269-17	18.50	101.70	179.44	0.57	0.0584	0.0013	0.6786	0.0159	0.0841	0.0007	0.0258	0.0004	546.3	50.0	525.9	9.6	520.7	4.2	514.8	8.4	98
L0269-18	8.62	49.71	82.54	0.60	0.0569	0.0019	0.6592	0.0230	0.0842	0.0009	0.0258	0.0006	487.1	78.7	514.1	14.1	521.0	5.2	513.9	11.0	98
L0269-19	14.79	120.97	133.69	0.90	0.0579	0.0017	0.6624	0.0191	0.0836	0.0007	0.0260	0.0004	524.1	64.8	516.1	11.6	517.6	4.4	518.0	8.7	99
L0269-20	12.44	91.20	115.60	0.79	0.0571	0.0015	0.6650	0.0192	0.0838	0.0008	0.0257	0.0004	498.2	59.3	517.7	11.7	518.7	4.8	512.3	8.5	99
L0269-21	11.40	66.19	107.74	0.61	0.0590	0.0017	0.6821	0.0193	0.0840	0.0009	0.0267	0.0005	564.9	63.0	528.0	11.6	520.0	5.2	533.1	9.7	98
L0269-22	9.26	68.98	82.16	0.84	0.0546	0.0019	0.6368	0.0216	0.0852	0.0009	0.0272	0.0005	394.5	77.8	500.3	13.4	526.8	5.4	542.6	10.2	94
L0269-23	13.50	97.73	124.98	0.78	0.0555	0.0016	0.6487	0.0191	0.0848	0.0008	0.0258	0.0004	435.2	63.0	507.7	11.7	524.8	4.9	514.9	8.1	96
L0269-24	7.05	42.53	67.69	0.63	0.0592	0.0024	0.6716	0.0270	0.0839	0.0010	0.0259	0.0007	572.3	90.7	521.7	16.4	519.1	6.0	516.6	13.2	99
L0269-25	12.51	66.65	120.70	0.55	0.0550	0.0015	0.6413	0.0175	0.0846	0.0008	0.0269	0.0005	413.0	61.1	503.1	10.9	523.6	4.6	537.4	10.4	96
L0269-26	6.33	42.89	58.21	0.74	0.0600	0.0026	0.6855	0.0284	0.0848	0.0010	0.0269	0.0007	611.1	97.2	530.1	17.1	524.7	6.2	535.7	12.8	98
L0269-27[2]	18.95	94.34	210.68	0.44	0.0625	0.0016	0.6300	0.0137	0.0731	0.0008	0.0307	0.0007	700.0	54.5	496.1	8.5	455.1	4.6	611.9	13.7	91
L0269-28[3]	7.64	50.60	73.08	0.69	0.0554	0.0025	0.6178	0.0271	0.0818	0.0009	0.0265	0.0007	427.8	100.0	488.5	17.0	507.1	5.2	529.0	12.9	96
L0269-29[3]	23.57	143.29	227.87	0.63	0.0581	0.0011	0.6568	0.0122	0.0820	0.0006	0.0256	0.0004	531.5	36.1	512.6	7.5	508.1	3.6	511.3	7.3	99
L0269-30	24.01	134.82	228.87	0.59	0.0572	0.0011	0.6652	0.0131	0.0842	0.0006	0.0259	0.0004	498.2	44.4	517.8	8.0	521.3	3.7	517.6	7.5	99
L0269-31	8.65	57.83	80.28	0.72	0.0594	0.0021	0.6761	0.0219	0.0837	0.0009	0.0264	0.0005	583.4	75.9	524.4	13.3	518.0	5.1	527.0	10.4	98
L0269-32	7.91	61.64	71.16	0.87	0.0561	0.0021	0.6423	0.0239	0.0840	0.0009	0.0263	0.0005	453.8	115.7	503.7	14.8	519.9	5.6	525.2	10.8	96

[1]Data not accepted because of abnormally high Th and U contents; [2]Concordance <95%; [3]The points that deducted by common of 204Pb correction.

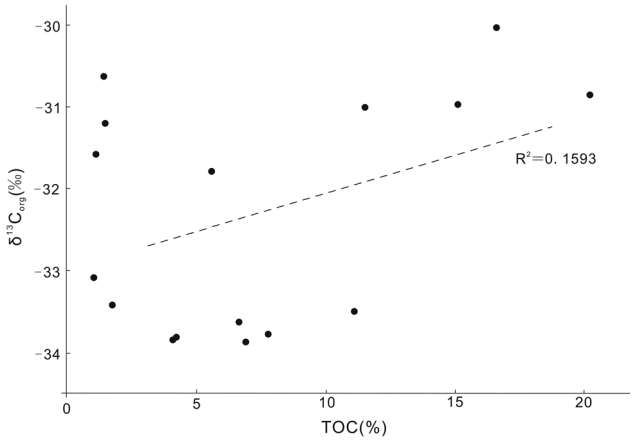

Figure 4: Cross-plot of $\delta^{13}C_{org}$ versus TOC contents of the Bagong section.

$\delta^{13}C$ isotope negative excursions have been identified during the early Cambrian in the Yangtze Platform. The first $\delta^{13}C$ negative excursion event, the basal Cambrian negative carbon isotope excursion (BACE), occurred before the small shelly fossil (SSF) assemblage zone of *Anabarites trisulcatus* appeared [44]. Since evidence of the BACE event has been found in many regions across the world, the BACE can be considered a sign of the beginning of the Cambrian [44,45], and it marks the extinction of the Ediacaran biota. The second negative $\delta^{13}C$ excursion event, called the Shiyantou negative carbon isotope excursion (SHICE), appears in the upper part of the second stage of the Cambrian and marks the boundary of the Terreneuvian and Series 2 [44]. Most studies suggest that this negative carbon isotope excursion is related to the rise in global sea level [44,46]. With the rise of sea level, upwelling of the deep anoxic seawater occurred and led to the extinction of the Small Shelly Biota [11]. Th is not sensitive to redox conditions, whereas U exists as U^{6+} that is soluble under oxic conditions and as insoluble U^{4+} in anoxic conditions, so U will become enriched in reduced sediments. Therefore, the Th/U ratio is higher in oxic conditions than in anoxic ones due to the release of U from sediment to seawater; in anoxic environments, the ratio is usually 0–2 [47]. An anoxic state was evident from the low Th/U ratios (<1) in the samples from the Bagong section.

There is a $\delta^{13}C$ positive excursion event between the two negative excursions, which corresponds to the SSF *Watsonella crosbyi* assemblage zone of the Zhujiaqing Formation in eastern Yunnan [11,48,49]. In South China, this positive excursion event is named the Zhujiaqing positive carbon isotope excursion (ZHUCE) [38]. The $\delta^{13}C$ positive excursion in this period has been discovered not only in Yangtze Platform but also in Siberia, Mongolia, and Morocco [50–53]. It can be used as a sign of the beginning of the second stage of the Cambrian [45].

As the water depth was greater in Sansui, Guizhou, than in Meishucun and Xiaotan, Yunnan, the sedimentation rate at Sansui may have been slower. Compared with shallow-water facies, a well-developed condensed

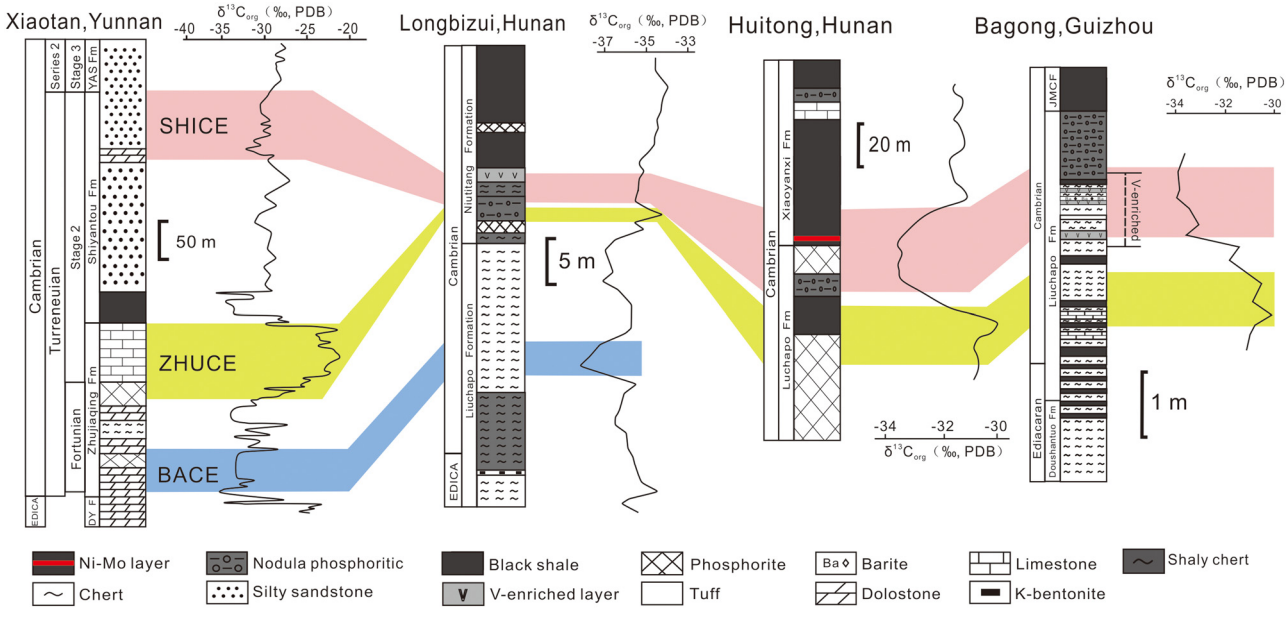

Figure 5: Carbon isotope chemostratigraphy of the Early Cambrian in the Yangtze region (modified after [46,49]). Section locations are illustrated in Figure 1. EDICA = Ediacaran; DY F = Dengying Formation; YAS F = Yu'anshan Formation; JMC F = Jiumenchong Formation.

section can be formed in Bagong [54,55]. There is a clear stratigraphic contact relationship in the Bagong deposit. The $\delta^{13}C_{org}$ data in the samples from the floor part of the deposit represent positive excursions. According to the lithostratigraphic correlation, the bottom of the Bagong deposit belongs to the Liuchapo Formation, and the positive excursions of $\delta^{13}C_{org}$ anomaly correspond to the ZHUCE. In the Bagong deposit, the tuff layer is in the middle of the V-enriched layer, and the $\delta^{13}C_{org}$ of this layer has a significant negative excursion. From the zircon U–Pb isotopic age of the tuff and the occurrence of phosphorous nodules at the top of the deposit, it can be inferred that the negative $\delta^{13}C_{org}$ excursion in the V-enriched layer corresponds to the SHICE event (see Figure 5).

The current evidence is not conclusive; however, based on comparisons of the ages of the tuff and K-bentonite in several sections of Yunnan, Hunan, and Guizhou, most researchers believe that the ZHUCE started at 532 Ma and ended at 522 Ma [23,56–58]. The lower boundary of the Bagong deposit should not be older than the start of the ZHUCE. The present study revealed a significant negative $\delta^{13}C_{org}$ excursion in the V-enriched layer, which corresponds to the SHICE found in Mo–Ni deposits in Hunan and eastern Yunnan [49,59,60]. As a sign of upwelling currents [61,62], phosphorus nodules are a consistent feature of the vanadium deposits as they are interbedded in the V-enriched layer. Their presence shows that upwelling currents occurred during the mineralization period of vanadium. In addition, the SHICE is considered to have been caused by the rise of anoxic water, and the upwelling currents of anoxic water led to the extinction of the Small Shelly Biota [12].

5.3 The age of the Liuchapo formation

The Liuchapo Formation is mainly composed of a set of strata of siliceous and carbonaceous rocks that represent the sediments of deep water to continental slope facies [25,63,64]. However, because reliable evidence from palaeontology and geochronology has been lacking, the age of Liuchapo Formation has been controversial. It is generally considered a diachronic stratum from the Ediacaran to the Cambrian.

An important event in the early Cambrian was the change of the marine environment from stratified to oxidizing [65]. The cause of this shift is still a matter of debate, but this change in the ocean environment may have been one of the main causes of the Cambrian explosion [66–70]. According to the mainstream views, the revolutionary evolution of life in the early Cambrian began in the shallow sea, so if the appropriate species could have settled in deep water, the deep sea would also have been oxidized [70]. The Liuchapo Formation represents a series of sediments that formed under deep water. Shallow-water fauna are hard to find in this formation because the life was limited by the stratified ocean environment. Therefore, biostratigraphic methods may be limited in the stratigraphic correlation of different facies belts in early Cambrian rocks. Geochemical marker layers that can be compared among different sections and isotopic ages are more accurate means for stratigraphic correlation.

The appearance of SSF is generally regarded as a sign of the beginning of the Cambrian [71,72]. Wang and Zhu discovered SSF in siliceous rocks and siltstone in the second member of the Liuchapo Formation, suggesting that the age of the upper Liuchapo Formation spanned the Cambrian [73]. Yang and Qian discovered abundant primitive pyramidal microfossils in dolomite from the first member of the Liuchapo Formation, suggesting that the bottom of the Liuchapo Formation may belong to the Ediacaran [63]. Therefore, based on evidence from palaeontology, the geological boundary between the Ediacaran and Cambrian in South China should be located in the lower part of the second member of the Liuchapo Formation or at the boundary between the first and second members. As a result of accurate U–Pb dating of zircons in different places of the world, the Precambrian-Cambrian boundary has been defined at 542 ± 1 Ma [74,75]. Chen et al. reported that the zircon SHRIMP ages of tuff from the Liuchapo Formation at the Bahuang section, Guizhou Province, and the Guanziping section, Hunan Province, were 542.6 ± 3.7 and 542.1 ± 5.0 Ma, respectively [76]. In another study, Chen et al. analysed the zircons U–Pb age (536 ± 5.5 Ma) of a tuff layer from Ganziping section, and the tuff may be related to a widespread volcanic activity occurred in South China at approximately 536 Ma [4]. This volcanic activity may be of great significance in the earth's history as the event that promoted the evolution of mollusks to animals with shells [14,77,78]. Recently, Wang et al. reported that new ages of the K-bentonite from the upper part of the Liuchapo Formation in the Pingyin section were measured by CA-ID-TIMS method. The ages of the K-bentonite in the middle and upper Liuchapo Formation were 541.48 ± 0.47 and 536.4 ± 0.47 Ma, respectively [79], and the stratum thickness between the K-bentonite layers (age 536.4 ± 0.47 Ma) and the bottom of the Niutitang Formation is more than 1 m. Therefore, the age of the middle Liuchapo Formation is not younger than 536 Ma and not older than 542 Ma.

The zircon U–Pb age of the vanadium deposit that occurred in Liuchapo Formation in Bagong section is obtained in the present study and is 520.9 ± 1 Ma. This age is approaching the boundary between the Cambrian Terreneuvian and Series 2; it is obviously younger than the age estimated of the middle part of the Liuchapo Formation (see Figure 6). The age of the V-enriched layer is close to the Mo–Ni layer at the bottom of the Niutitang Formation that was determined by Zhou et al. (521 ± 5 Ma) and Xu et al. (521 ± 5 Ma) [14,22]. Thus, the middle-upper Liuchapo Formation in eastern Guizhou may represent the same epoch as the bottom of the Niutitang Formation in northern Guizhou. The reason for this phenomenon may be that eastern Guizhou is in a deep-water sedimentary environment, the sediment phase change from northern to eastern Guizhou. This shows that lithostratigraphic correlation is not accurate in early Cambrian. Because of the absence of palaeontological fossils, the stratigraphic time obtained from lithology of the lower Cambrian strata in South China is less reliable than that obtained using geochemical markers.

The tuff in the Bagong vanadium deposit, Sansui, is located in the middle of the V-enriched layer (see Figure 2a), The V-enriched layer is an ideal geochemical marker that can be observed in many sections in South China [10,17,18,20]. The zircon U–Pb age of the tuff in Bagong deposit should represent the age of the V-enriched layers in eastern Guizhou and even South China. The upper part of the Liuchapo Formation belongs to the Cambrian System. In Bagong section, the age of V-enriched layer is same with Mo–Ni-enriched layer in the bottom of Niutitang Formation in northern Guizhou; the difference of lithostratigraphy is caused by sedimentary phase change.

5.4 Metallogenic age of V–Mo–Ni–PGE deposits in South China

The Mo–Ni–V–PGE-enriched layer of South China is found in lower Cambrian black shales. This mineralized belt can be traced along the same stratigraphic horizon over distances up to 2,000 km [22]. This stratigraphic horizon can be used as an important geochemical marker layer for the division and comparison of the lower Cambrian rocks in South China [16,59,60].

There are many deposits (ore spots) in this belt, such as those in Songlin, Ganziping, and Huitong, in which Mo and Ni are main ore-forming elements. However, in some other sections, such as Sansui and Jiangkou, V is the main metallogenic element [20]. Some scholars believe that the Mo–Ni and V deposits formed in the

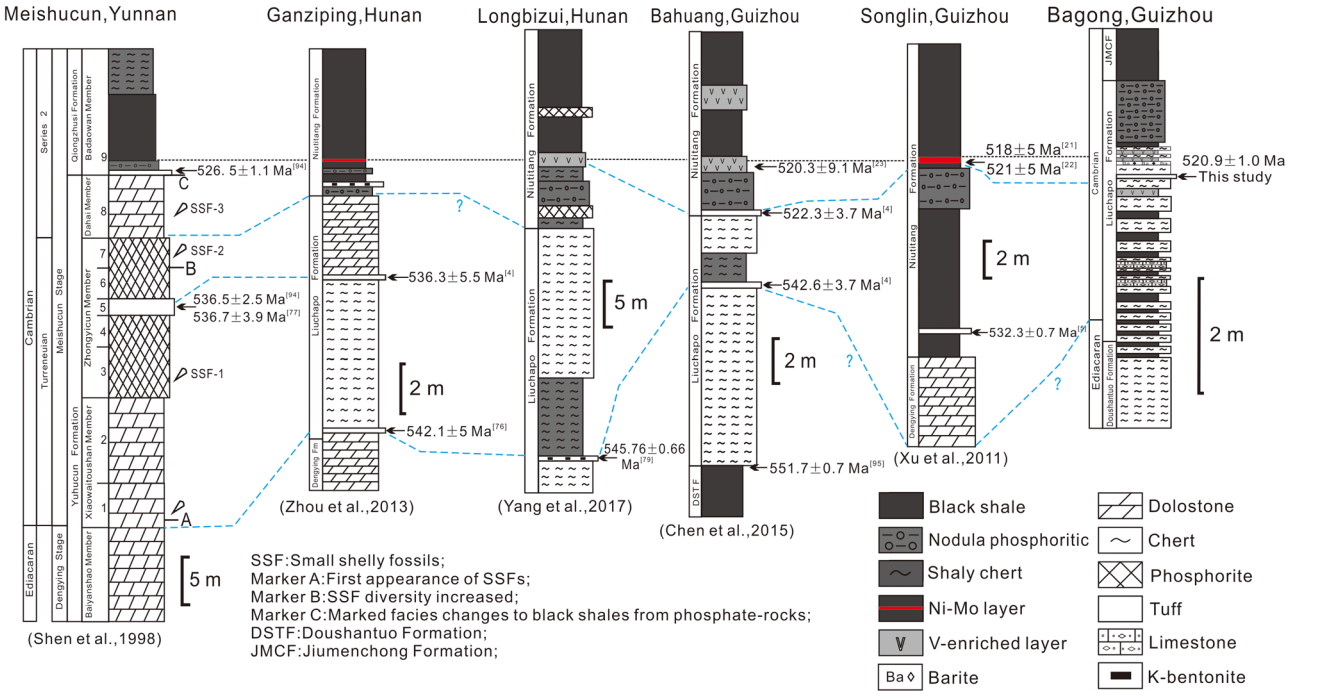

Figure 6: Stratigraphic columns of the Late Ediacaran-Early Cambrian boundary successions in the Yangtze Platform, South China, constrained by isotope ages (modified after [4,5,14,21,22,54,76,93–96]). Section locations are illustrated in Figure 1.

same period and that the differentiation of mineral elements is controlled by paleogeography and marine redox conditions [38,39,54]. There is also the view that the formation age of the V deposits is earlier than that of the Mo–Ni deposits [80]. The Mo–Ni-enriched layer is a geochemical marker layer, not only in South China but also elsewhere. Based on a study of Mo isotopic composition in Hunan and Morocco, Wille et al. concluded that the worldwide anoxic upwelling in the early Cambrian induced the formation of the Mo–Ni–V–PGE deposits and then led to the extinction of the Ediacaran biota [12,81]. Some studies mentioned that the sedimentary rate is low in anoxic environments and is conductive to the deposition and preservation of metal elements [22,82,83]. The low sedimentary rate of the upper Liuchapo Formation was caused by the sea level rise [22]. Although the views of the age of Mo–Ni–V–PGE are not completely unified, most researchers agree that the formation of Mo–Ni polymetallic deposits was induced by the oceanic anoxic events [22,63,82,84]. As the anoxic upwelling current flowed from the basin to the slope, V deposits that formed in deep water can represent the age of marine environment transformation better than Mo–Ni deposits.

In the 1990s, Horan et al. conducted the first Re-Os dating study of the lower Cambrian Ni-Mo polymetallic layer on the Yangtze Platform and determined its age as 560 ± 50 Ma [85]. Since the beginning of the 21st century, different scholars have successively performed isotope dating studies on this layer. Wille et al. got the age of Ni–Mo-bearing polymetallic layer as 541 ± 16 Ma, and they regarded this layer as a horizon at the Precambrian-Cambrian boundary comparable to the volcanic ash beds in the A4 carbonate rocks in the bottom of the Ara Group, Oman (U–Pb age of 541 ± 0.13 Ma) [12]. That is the internationally recognized marker beds of the Precambrian-Cambrian boundary. Through the studies of Ni–Mo–PGE sulfide beds in South China, Li et al. [86] and Jiang et al. [87] obtained Re-Os isochron ages of 542 ± 11 and 537 ± 10 Ma, respectively. However, authors of some later studies subsequently questioned Wille's global comparison scheme through zircon SHRIMP U–Pb dating and regional stratigraphic correlation studies on the volcanic ash layers from the bottom of the Niutitang Formation [5,88]. In the early studies, although the ages of Ni–Mo-bearing polymetallic layers are consistent, the analytical accuracy is low. Recently, Xu et al. reported that the Re-Os isochron age of the Ni–Mo-bearing polymetallic layer is 521 ± 5 Ma, which is the highest-precision Re-Os isochron age obtained thus far [22].

The zircon SHRIMP U–Pb age of K-bentonites at the bottom of the Niutitang Formation in the Jianpo section of Songlin, Zunyi, reported by Zhou et al. is 518 ± 5 Ma [21]. Later, Jiang et al. applied zircon SHRIMP U–Pb dating to the same layers of K-bentonites and obtained an age of 532.3 ± 0.7 Ma [5]. Zhou et al. considered the age of the Mo–Ni-bearing strata to be less than 536 ± 5 Ma after the study on the K-bentonites overlying the Laobao Formation in Jiangkou, Guizhou Province [14]. Chen et al. obtained ages of 524.2 ± 5.1 and 522.3 ± 3.7 Ma measured at the top of the Liuchapo Formation, western Hunan, and considered these ages to be close to or slightly earlier than the formation of the Mo–Ni and V-enriched layers [76]. In a study of Re-Os isotopic data from the metalliferous deposits in the lower part of the Niutitang Formation, Fu et al. concluded that the age of the V-enriched layer was 520.3 ± 9.1 Ma [23]. This age is closed with the conclusion of present study.

In addition to studies of isotopic absolute age, some researches establishing stratigraphic correlations have been conducted by comparisons with the variable characteristics of carbon and oxygen isotopes [30,53,89–91]. The Zhujiaqing-Shiyantou Formation in Yunnan, which corresponds to the Liuchapo-Niutitang Formation in Guizhou, records an obvious positive $\delta^{13}C$ excursion, which can be globally correlated. The age of the positive $\delta^{13}C$ excursion event is 525.34 ± 0.09 Ma in the lower Cambrian rocks of Morocco [53,91]. Therefore, the bottom age of the Niutitang Formation should not be less than 525 Ma.

A direct and feasible method of stratigraphic correlation for the lower Cambrian strata that is lacking of biological fossils is to use absolute age data. Most studies about the age of Mo–Ni–V–PGE-enriched layer are focused on Mo–Ni deposits; however, whether the genesis of V deposit is consistent with that of Mo–Ni deposits is still controversial. For this reason, a direct age evidence from V deposit would be an important evidence to prove that the V deposit and Mo–Ni deposits were formed at the same metallogenic period. In the Bagong vanadium deposit, the tuff is directly intercalated into the V-enriched layer with clear contact relationship. Therefore, the zircon U–Pb age of the tuff can accurately reflect the age of the vanadium deposit. The zircon U–Pb age of Bagong vanadium deposit is 520.9 ± 1 Ma, which is close to the age of Mo–Ni deposits in other sections in South China. This similarity means that these Mo–Ni–V deposits in south China may have formed in the same metallogenic event.

Some additional studies emphasized that the formation of the Mo–Ni and V deposits in South China was mainly restricted by marine chemical conditions [17,18,54,92].

The V deposits were formed in the bottom to middle of the continental slope, while the Mo–Ni deposits were mainly formed in the upper continental slope and the shelf. A significant event in the early Cambrian caused the global oceans to change from anoxic to oxic [93]. Some environmental fluctuations occurred during this process, but the time interval coincided with the metallogenic period of Mo–Ni–V–PGE deposits in South China. The V^+ can form the stable oxides in oxidation environment because the lower Cambrian vanadium deposits in South China are mostly located in the lower or middle part of the continental slope facies, indicating that the V^+ formed stable oxides in the oxidation environment. Therefore, the vanadium deposits may have been formed before the ocean oxidation event. These observations indicate that the complete oxidation time of the ocean should not be earlier than the formation of the vanadium deposits at approximately 521 Ma.

Studies on the $\delta^{13}C_{org}$ in other sections of Yangtze platform have shown that the age of SHICE is consistent with the Mo–Ni layer [28,32,55,58,90]. The $\delta^{13}C_{org}$ evidence from Sansui indicates that the SHICE is related to the formation of V deposits. Thus, the age of the V deposits and the Mo–Ni deposits should be very close or the same.

6 Conclusion

Based on the analysis of zircon U–Pb age and the stratigraphic correlation based on $\delta^{13}C_{org}$ values, the upper part of the Liuchapo Formation in eastern Guizhou belongs to the Cambrian. The age of the vanadium deposits is approximately 521 Ma, which is close to the boundary between the Terreneuvian and Series 2 of the Cambrian. This age coincides with the time when the global marine environment changed from anoxic to oxic in the early Cambrian. The organic carbon isotope data from the V-enriched layer are comparable to those of SHICE; this negative carbon isotope excursion event corresponds to the upper part of the Cambrian Stage 2.

The ages of the Mo–Ni polymetallic layer and V deposits in South China are very similar and both reflect the early Cambrian changes in the marine environment. Because V deposits were mainly formed in deep water, when the upwelling current was enhanced by anoxic seawater from the depths, the formation of the V deposits may have occurred slightly earlier than that of the Mo–Ni deposits, which formed mainly in shallow-water in response to environmental changes. The ages of the metallogenic times between the Mo–Ni and V deposits are very close, which means that these deposits should be attributed to the same metallogenic event.

The Mo–Ni–V-enriched layer is an important geochemical marker for identifying lower Cambrian strata, but it is only limited to the shallow-water facies in South China. However, the V-enriched layer could be a new geochemical marker to identify lower Cambrian strata in continental slope facies.

Acknowledgements: The authors thank Dr Jun Chen (Institute of Geochemistry, Chinese Academy of Sciences) and Liang Li (Nanjing FocuMS Technology Co., Ltd) for providing help with testing and data analysis.

Funding information: This research was funded by the Talent Innovation Team Foundation of Guizhou Science and Technology Department, grant number QKHRC[2018] 5613 and National Natural Science Foundation of China [No. 41890841].

Author contributions: Tong Wu and Ruidong Yang designed the experiments, and Tong Wu carried them out. Junbo Gao provided some suggestions for manuscript preparation. Tong Wu and Jun Li conducted field sampling. Tong Wu prepared the manuscript with contributions from all co-authors. The authors applied the SDC approach to determine the sequence of authors. All the authors listed have approved the manuscript that is enclosed.

Conflict of interest: The authors declare no conflict of interest. No conflict of interest exists in the submission of this manuscript, and manuscript has been approved by all authors for publication. I would like to declare on behalf of my co-authors that the work described is original research that has not been published previously and is not under consideration for publication elsewhere, in whole or in part.

References

[1] Steiner M, Wallis E, Erdtmann BD, Zhao YL. Submarine-hydrothermal exhalative ore layers in black shales from South China and associated fossils-insights into a Lower Cambrian facies and bio-evolution. Palaeogeogr Palaeocl. 2001;169(3–4):165–91.

[2] Chen JY, Huang DY. A possible Lower Cambrian Chaetognath (arrow worm). Science. 2002;298(5591):187.

[3] Hou XG, Siveter DJ, Aldridge RJ, Siveter DJ. Collective behavior in an early Cambrian arthropod. Science. 2008;322(5899):224.

[4] Chen DZ, Wang JG, Qing HR, Yan D, Li R. Hydrothermal venting activities in the early Cambrian, South China: petrological, geochronological and stable isotopic constraints. Chem Geol. 2009;258(3–4):168–81.
[5] Jiang SY, Pi DH, Heubeck C, Feimmel H, Liu YP, Deng HL, et al. Early Cambrian ocean anoxia in South China. Nature. 2009;459:E5–6.
[6] Zhou C, Jiang SY. Palaeoceanographic redox environments for the lower Cambrian Hetang formation in South China: evidence from pyrite framboids, redox sensitive trace elements, and sponge biota occurrence. Palaeogeogr Palaeocl. 2009;271:279–86.
[7] Briggs DEG. Palaeontology: decay distorts ancestry. Nature. 2010;463:741–3.
[8] Pasava J, Frimmel H, Luo TY, Koubová M, Martínek K. Extreme PGE concentrations in lower Cambrian acid tuff layer from the Kunyang phosphate deposit, Yunnan province, South China-Possible PGE source for lower Cambrian Mo–Ni-polyelement ore beds. Econ Geol. 2010;105:1047–56.
[9] Fu Y, Sun T. PGE geochemical characteristics of the Huangshanxi magmatic Ni-Cu sulfide deposit, East Tianshan, Xinjiang,and its significance for the mineralization. Adv Mater Res. 2014;164:962–5.
[10] Jiang XJ, Wang SS. An analysison geological characteristics and genesis of Qingmugou vanadium deposit in Yunxian of Hubei. Miner Resour Geol. 2016;30:774–7.
[11] Steiner M, Li G, Qian Y, Zhu M, Erdtmann BD. Neoproterozoic to early Cambrian small shelly fossil assemblages and a revised biostratigraphic correlation of the Yangtze Platform (China). Palaeogeogr Palaeocl. 2007;254(1–2):67–99.
[12] Wille M, Nägler TF, Lehmann B, Stefan SS, Jan D, Kramers JD. Hydrogen sulphide release to surface waters at the Precambrian/Cambrian boundary. Nature. 2008;453:767–9.
[13] Li D, Ling HF, Jiang SY, Pan JY, Chen YQ, Cai YF, et al. New carbon isotope stratigraphy of the Ediacaran-Cambrian boundary interval from SW China: implications for global correlation. Geol Mag. 2009;146(4):465–84.
[14] Zhou MZ, Luo TY, Liu SR, Qian ZK, Xing LC. SHRIMP zircon age for a K-bentonite in the top of the Laobao formation at the Pingyin section, Guizhou, South China. Sci China Ser D. 2013;43:1195–1206.
[15] Zi JP, Jia D, Wei GQ, Yang ZY, Zhang Y, Hu J, et al. LA-ICP-MS U–Pb Zircon ages of volcaniclastic beds of the third member of the Sinian (Ediacaran) Dengying formation in Leshan, Sichuan, and a discussion on the rift evolution in the basin. Geol Rev. 2017;63:1040–9.
[16] Coveney RM, Nansheng C. Ni–Mo–PGE–Au-rich ores in Chinese black shales and speculations on possible analogs in the United-States. Min Depos. 1991;26(2):83–8.
[17] You XJ, Sun JM, Chen MH, Bao ZX, Bao JM. V deposit in Lower Cambrian black rock series of northwestern Hunan. Min Resour Geol. 2008;22:20–6.
[18] Hu NY, Xia HD, Dai TG, You XJ, Bao ZX, Bao JM. Sedimentary vanadium deposit of lower Cambrian black rock series in west Hunan . Contrib Geol Miner Res Res. 2010;25:296–302.
[19] Li J, Gao JB, Wei HR, Chen SY, Wu T, Gao L, et al. Divison and contrast of metallogenic Sequence in the Base of Cambrian black rock series in Guizhou province. Geol Prospec. 2019;55(2):508–18.
[20] Wei HR, Yang RD, Gao JB. The mineralization processes of hydrothermal sedimentary deposits in basal Cambrian black shales from Guizhou provience. China: Guizhou Science and Technology Publishing House; 2017.
[21] Zhou MZ, Luo TY, Li ZX, Zhao H, Long HS, Yang Y. Zircons SHRIMP U–Pb ages and its geological significance from Tuff at the bottom of Niutitang formation, Zunyi, Guizhou. China Sci Bull. 2008;53(4):576–83.
[22] Xu LG, Bernd L, Mao JW, Qu WJ, Du AD. Re-Os age of polymetallic Ni–Mo–PGE–Au mineralization in early Cambrian black shales of South China-A reassessment. Econ Geol. 2011;106:511–22.
[23] Fu Y, Dong L, Li C, Qu W, Pei HX, Qiao WL, et al. New Re-Os Isotopic Constrains on the formation of the metalliferous deposits of the lower Cambrian Niutitang formation. J Earth Sci. 2016;27(2):271–81.
[24] Zhu MY, Zhang JM, Steiner M, Yang AH, Li GX, Erdtmann BD. Sinian-Cambrian stratigraphic framework for shallow-to deep-water environments of the Yangtze Platform: an integrated approach. Prog Nat Sci. 2003;13:951–60.
[25] Wang Y, Huang ZQ, Chen HD, Hou MC, Yang YF, Du BY. Stratigraphical correlation of the Liuchapo formation with the Dengying formation in South China. J Jilin Univ (Earth Sci Ed). 2012;42:328–35.
[26] Jiang G, Shi X, Zhang S, Wang Y, Xiao S. Stratigraphy and paleogeography of the Ediacaran Doushantuo formation (ca. 635–551Ma) in South China. Gondwana Res. 2011;19:831–49.
[27] Hu ZC, Gao S, Liu YS, Hu S, Chen H, Yuan H. Signal enhancement in laser ablation ICP-MS by addition of nitrogen in the central channel gas. J Anal Spectrom. 2008;23:1093–101.
[28] Mao J, Lehmann B, Du A, Zhang G, Ma D, Wang Y, et al. Re-Os dating of polymetallic Ni–Mo–PGE–Au mineralization in lower Cambrian black shales of South China and its geologic significance. Econ Geol. 2002;17(5):1535–47.
[29] Liu YS, Gao S, Hu ZC, Gao CG, Zong KQ, Wang DB. Continental and oceanic crust recycling-induced melt-peridotite interactions in the trans-north China Orogen: U–Pb dating, Hf isotopes and trace elements in zircons from mantle xenoliths. J Pet. 2010;51:537–71.
[30] Liu YS, Hu ZC, Zong KQ, Gao CG, Gao S, Xu J, et al. Reappraisement and refinement of zircon U–Pb isotope and trace element analyses by LA-ICP-MS. Chin Sci Bull. 2010;55:1535–46.
[31] Ludwig K. Geochronological toolkit for microsoft excel. Isoplot. 2003;3:1–70.
[32] Klötzli U, Klötzli E, Günes Z, Kosler J. Accuracy of laser ablation U–Pb zircon dating: results from a test using five different reference zircons. Geostand Geoanalyt Res. 2009;33(1):5–15.
[33] Li XH, Liu XM, Liu YS, Su L, Sun WD, Huang HQ, et al. Accuracy of LA-ICPMS zircon U–Pb age determination: an inter-laboratory comparison. Sci China Earth Sci. 2015;58(10):1722–30.
[34] Li YG, Wang SS, Liu MW, Meng E, Wei XY, Zhao HB, et al. U–Pb dating study of baddeleyite by LA-ICP-MS: technique and application. Acta Geol Sin. 2015;12:2400–18.
[35] Qiu LJ, Huang GL, Shuai Q, Su Y. Reconstruction of the conversion relationship between organic matter and total organic carbon in calcination method and its application in shale analysis. Rock Min Anal. 2015;34(2):218–23.
[36] Stacey JS, Kramers JD. Approximation of terrestrial lead isotope evolution by a two-stage model. Earth Planet Sc Lett. 1975;26(2):207–22.

[37] Hatcher PG, Spiker EC, Szeverenyi NM, Maciel GE. Selective preservationand origin of petroleum-forming aquatic kerogen. Nature. 1983;305(5394):498–501.
[38] Marshall JD. Climatic and oceanographic isotopic signals from the carbonate rock record and their preservation. Geol Mag. 1992;129(2):143–60.
[39] Altabet MA, Francois R. Sedimentary nitrogen isotopic ratio as a recorder for surface ocean nitrate utilization. Glob Biogeochem Cy. 1994;8(1):103–16.
[40] Freudenthal T, Wagner T, Wenzhöfer F, Zabel M, Wefer G. Early diagenesis of organic matter from sediments of the eastern subtropical Atlantic: evidence from stable nitrogen and carbon isotopes. Geochim Cosmochim Ac. 2001;65(11):1795–808.
[41] Galimov EM. The pattern of delta ^{13}C(org) versus HI/OI relation in recent sediments as an indicator of geochemical regime in marine basins: comparison of the Black Sea, Kara Sea, and Cariaco trench. Chem Geol. 2004;204(3–4):287–301.
[42] Peters KE, Rohrback BG, Kaplan IR. Carbon and hydrogen stable isotope variations in kerogen during laboratory-simulated thermal maturation. AAPG Bull. 1981;65(3):501–8.
[43] Schwab V, Spangenberg JE, Grimalt JO. Chemical and carbon isotopic evolution of hydrocarbons during prograde metamorphism from 100°C to 550°C: case study in the Liassic black shale formation of Central Swiss Alps. Geochim Cosmochim Ac. 2005;69(7):1825–40.
[44] Zhu MY, Babcock LE, Peng SC. Advances in Cambrian stratigraphy and paleontology: integrating correlation techniques, paleobiology, taphonomy and paleoenvironmental reconstruction. Palaeoworld. 2006;15:217–22.
[45] Zhu MY, Yang AH, Yuan JL, Li GX, Zhang JM, Zhao FC, et al. Cambrian integrative stratigraphy and timescale of China. Sci China Earth Sci. 2019;62:25–60.
[46] Wang D, Ling HF, Ulrich S, Yao SP, Li D, Wei W, et al. Organic carbon isotope stratigraphy of the early Cambrian Huitong section in Hunan Province, South eastern Yangtze, China. Geol J China Univ. 2016;22(2):274–88.
[47] Wignall PB, Twitchett RJ. Oceanic anoxia and the end Permian mass extinction. Science. 1996;272(5265):1155–8.
[48] Li G, Xiao S. Tannuolina and Micrina (Tannuolinidae) from the lower Cambrian of eastern Yunnan, South China, and their scleritome reconstruction. J Paleontol. 2004;78(5):900–13.
[49] Cremonese L, Shields-Zhou G, Struck U, Ling HF. Marine biogeochemical cycling during the early Cambrian constrained by a nitrogen and organic carbon isotope study of the Xiaotan section, South China. Precambrian Res. 2013;225:148–65.
[50] Brasier MD, Shields G, Kuleshov VN, Zhegallo EA. Integrated chemo and biostratigraphic calibration of early animal evolution: neoproterozoic-early Cambrian of southwest Mongolia. Geol Mag. 1996;133(04):445–85.
[51] Kaufman AJ, Knoll AH, Semikhatov MA, Grotzinger P, Jacobsen SB, Adams W. Integrated chronostratigraphy of Proterozoic-Cambrian boundary beds in the western Anabar region, northern Siberia. Geol Mag. 2006;133(5):509–33.
[52] Maloof AC, Schrag DP, Crowley JL, Bowring SA. An expanded record of early Cambrian carbon cycling from the Anti-Atlas margin, Morocco. Can J Earth Sci. 2005;42(12):2195–216.
[53] Maloof AC, Ramezani J, Bowring SA, Fike DA, Porter SM, Mazouad M. Constraints on early Cambrian carbon cycling from the duration of the Nemakit-Daldynian-Tommotian boundary δ13C shift, Morocco. Geology. 2010;38(7):623–6.
[54] Cisne JL, Gildner RF, Rabe BD. Epeiric sedimentation and sea level, synthetic ecostratigraphy. Lethaia. 1984;17:267–88.
[55] Xu GR. Relationships of sea-level change with water depth change and sedimentation rate in epeiric sea. Geol Sci Tech Info. 1992;11(3):31–4.
[56] Guo QJ, Strauss H, Liu CQ, Goldberg T, Zhu MY, Pi DH, et al. Carbon isotopic evolution of the terminal neoproterozoic and early Cambrian: evidence from the Yangtze platform, South China. Palaeogeogr Palaeocl. 2007;254(1–2):140–57.
[57] Guo QJ, Strauss H, Zhu MY, Zhang JM, Yang XL, Lu M, et al. High resolution organic carbon isotope stratigraphy from a slope to basinal setting on the Yangtze Platform, South China: implications for the Ediacaran-Cambrian transition. Precambrian Res. 2013;225:209–17.
[58] Wang J, Chen D, Yan D, Wei HY, Xiang L. Evolution from an anoxic to oxic deep ocean during the Ediacaran-Cambrian transition and implications for bioradiation. Chem Geol. 2012a;306–307:129–38.
[59] Och LM, Shields-Zhou GA, Poulton SW, Manning C, Thirlwall MF, Li D, et al. Redox changes in early Cambrian black shales at Xiaotan section, Yunnan Province, South China. Precambrian Res. 2013;225:166–89.
[60] Wang D, Struck U, Ling HF, Guo QJ, Shields-Zhou GA, Zhu MY, et al. Marine redox variations and nitrogen cycle of the early Cambrian southern margin of the Yangtze Platform, South China: evidence from nitrogen and organic carbon isotopes. Precambrian Res. 2015;267:209–26.
[61] Baturin GN. The origin of marine phosphorites. Int Geol Rev. 1989;31:327–42.
[62] Zhou WX, Wang HJ, Fu Y. Study on the formation mechanism of phosphate nodules in the early Cambrian period using LA-ICP-MS multi-element imaging technology. Rock Miner Anal. 2017;36(2):97–106.
[63] Yang RD, Qian Y. Microfossils from the Dengying formation of Wuhe section, Taijiang county, Guizhou province. Chin J Geol. 2005;40(1):40–6.
[64] Zhu MY, Strauss H, Shields GA. From snowball earth to the Cambrian bioradiation: calibration of Ediacaran-Cambrian earth history in South China. Palaeogeogr Palaeocl. 2007;254(1–2):1–6.
[65] Canfield DE. A new model for Proterozoic ocean chemistry. Nature. 1998;396(6710):450–3.
[66] Scott C, Lyons TW, Bekker A, Shen Y, Poulton SW, Chu X, et al. Tracing the stepwise oxygenation of the Proterozoic ocean. Nature. 2008;452(7186):456–9.
[67] Sahoo SK, Planavsky NJ, Kendall B, Wang X, Shi X, Scott C, et al. Ocean oxygenation in the wake of the marinoan glaciation. Nature. 2012;489(7417):546–9.
[68] Chen X, Ling HF, Vance D, Zhou GS, Zhu MY, Poulton SW, et al. Rise to modern levels of ocean oxygenation coincided with the Cambrian radiation of animals. Nat Commun. 2015;2017(3):210–20.
[69] Dahl TW, Connelly JN, Kouchinsky A, Gill BC, Manssonet SF, Bizzarro M. Reorganisation of earth's biogeochemical cycles briefly oxygenated the oceans 520 Myr ago. Geochem Perspect Let. 2017;3(2):210–20.

[70] Wang D, Ling HF, Struck U, Zhu XK, Zhu M, He T, et al. Coupling of ocean redox and animal evolution during the Ediacaran-Cambrian transition. Nat Commun. 2018;2575(9):1–8.
[71] Brasier M, Cowie J, Taylor M. Decision on the Precambrian-Cambrian boundary stratotype. Episodes. 1994;17(1–2):3–8.
[72] Yin GZ. Division and correlation of Cambrian in Guizhou. Guizhou Geol. 1996;47:115–28.
[73] Wang YG, Zhu SX. New progress in the research of phosphorus-bearing strata and phosphorites in Doushamntuo formation, central Guizhou. Regional Geol China. 1984;1:129.
[74] Amthor JE, Grotzinger JP, Schroder S, Bowring SA, Matter A. Extinction of Cloudina and Namacalathus at the Precambrian-Cambrian boundary in Oman. Geology. 2003;31(5):431–4.
[75] Bowring SA, Grotzinger JP, Condon DJ, Ramezani J, Newall MJ, Allen PA. Geochronologic constraints on the chronostratigraphic framework of the Neoproterozoic Huqf Supergroup, sultanate of Oman. Am J Sci. 2007;307(10):1097–145.
[76] Chen DZ, Zhou XQ, Fu Y, Wang JG, Yan DT. New U–Pb zircon ages of the Ediacaran-Cambrian boundary strata in South China. Terra Nova. 2015;27(1):62–8.
[77] Zhu RX, Li XH, Hou XG, Pan YX, Wang F, Deng CL, et al. SIMS U–Pb zircon age of a tuff layer in the Meishucun section, Yunnan, southwest China: constraint on the age of the Precambrian-Cambrian boundary. Sci China Ser D. 2009;39:1105–11.
[78] Yang EL, Lv XB, Shi P, Wu B, Liu W, Ding YN. Detrital zircon age of stratigraphic Sinian-Cambrian in east Guizhou and its geological significance. J China Univ Geosci. 2014;39(4):387–98.
[79] Wang W, Zhou M, Chu Z, Xu J, Li C, Luo T, et al. Constraints on the Ediacaran-Cambrian boundary in deep-water realm in South China: evidence from zircon CA-ID-TIMS U–Pb ages from the topmost Liuchapo Formation. Sci China Earth Sci. 2020;50(6):819–31.
[80] Pi DH. Geochemistry of early Cambrian black rock series from Zunyi, Guizhou Province. PhD thesis, China: Geochemistry Chinese Academy of Sciences; 2007.
[81] Bamhach RK. Phanerozoic biodiversity mass extinctions. Annu Rev Earth Pl Sci. 2006;34:127–55.
[82] Stein R. Organic carbon content/sedimentation rate relationship and its paleoenvironmental significance for marine sediments. Geo-Mar Lett. 1990;10:37–44.
[83] Lehmann B, Nägler TF, Holland HD, Wille M, Mao J, Pan J, et al. Highly metalliferous carbonaceous shale and early Cambrian seawater. Geology. 2007;35:403–6.
[84] Lan Z, Li XH, Chu X, Tang G, Yang S, Yang H, et al. SIMS U–Pb zircon ages and Ni–Mo–PGE geochemistry of the lower Cambrian Niutitang formation in South China: constraints on Ni–Mo–PGE mineralization and stratigraphic correlations. J Asian Earth Sci. 2017;137(15):141–62.
[85] Horan MF, Morgan JW, Grauch RI, Coveney RM, Murowchick JB, Hulbert LJ. Rhenium and Osmium isotopes in black shales and Ni–Mo–PGE-rich sulfide layers, Yukon Territory, Canada, and Hunan and Guizhou provinces, China. Geochim Cosmochim Acta. 1994;58(1):257–65.
[86] Li SR, Xiao QY, Shen JF, Sun L, Liu B, Yan BQ. Re-Os isotopic constraints on the origin and mineralization age of platinum group elements in the lower Cambrian of Hunan and Guizhou. Sci China (Ser D). 2002;32(7):568–75.
[87] Jiang S, Yang J, Ling H, Feng H, Chen Y, Chen J. Re-Os isotopes and PGE geochemistry of black shales and intercalated Ni-Mo polymetallic sulfide bed from the Lower Cambrian Niutitang Formation, South China. Prog Nat Sci. 2003;13:788–94.
[88] Wen HJ, Zhang YX, Fan HF, Hu RZ. Mo isotopes in the lower Cambrian formation of southern China and its implications on paleo-ocean environment. Chin Sci Bull. 2009;54(24):4756–62.
[89] Shen Y, Schidlowski M. New C isotope stratigraphy from southwest China: implications for the placement of the Precambrian-Cambrian boundary on the Yangtze Platform and global correlations. Geology. 2000;28:623–6.
[90] Zhou CM, Zhang JM, Li GX, Yu ZZ. Carbon and oxygen isotopic record of the early Cambrian from the Xiaotan section, Yunnan, South China. Sci Geol Sin. 1997;32(2):201–11.
[91] Sawaki Y, Nishizawa M, Suo T, Komiya T, Hirata T, Takahata N, et al. Internal structures and U–Pb ages of zircons from a tuff layer in the Meishucunian formation, Yunnan Province, South China. Gondwana Res. 2008;14(1–2):148–58.
[92] Shang FH, Zhu YM, Hu QH, Wang Y, Li Y, Li W, et al. Factors controlling organic-matter accumulation in the upper Ordovician-lower Silurian organic-rich shale on the northeast margin of the upper Yangtze platform: evidence from petrographic and geochemical proxies. Mar Pet Geol. 2020;121:104597. doi: 10.1016/j.marpetgeo.2020.104597.
[93] Xiang L, Cai CF, He XY, Jiang L, Yuan YY, Wang TK, et al. Ocean redox state evolution and its controlling factors during Cambrian Terreneuvian epoch:evidence from Lijiatuo section, south China. J China Univ Geosci. 2015;40:1197–214.
[94] Compston W, Zhang Z, Cooper JA, Ma G, Jenkins RJF. Further shrimp geochronology on the early cambrian of south china. Am J Sci. 2008;308(4):399–420.
[95] Yang C, Zhu MY, Condon DJ, Li XH. Geochronological constraints on stratigraphic correlation and oceanic oxygenation in Ediacaran-Cambrian transition in South China. J Asian Earth Sci. 2017;140:75–81.
[96] Condon D, Zhu MY, Bowring S, Wang W, Yang AH, Jin YG. U–Pb Ages from the Neoproterozoic Doushantuo formation, China. Science. 2005;308(5718):95–8.